Flame characteristics of glycerol/methanol blends in a swirl-stabilised gas turbine burner

Ogbonnaya Agwu[a,*], Agustin Valera-Medina[a], Tomaz Katrasnik[b], Tine Seljak[b]

[a]*School of Engineering, Cardiff University, CF24 3AA, Cardiff, UK*

[b]*Faculty of Mechanical Engineering, University of Ljubljana, Ljubljana, Slovenia*

*Corresponding author. Email: AgwuOE@cardiff.ac.uk

Abstract

Finding alternative value-added usage for glycerol is imperative as existing uses are inadequate due to the vast excesses of glycerol generated mainly as a result of increased biodiesel production. This paper explores a mid-term, cost-efficient, technically viable utilisation in power generation applications and exposes the nature of its combustion. Blended with methanol to avoid the heat loss and fuel coking problems associated with preheating, glycerol was combusted in a model swirl-stabilised gas turbine burner utilising a standard pressure-swirl injector for fuel atomisation. Stable flames resulting from the tested blends – 70/30 and 50/50 combinations of methanol/glycerol by volume – were achieved over an equivalence ratio (ER) range between 0.29 and 0.51. The upper and lower limits of stable operating ER for the 70/30 case were accompanied by significant flame lift-off from the nozzle exit orifice – a phenomenon that was not pronounced in the 50/50 case. Also, the temporal variation of CH* species integral intensity suggested a reduction in the fluctuation of heat release rate, hence better flame stability, as ER increased for both blends. Overall, the 50/50 case showed greater flame stability compared with the 70/30 case based on the CH* chemiluminescence data and spectral analysis by means of fast Fourier transform.

Keywords: glycerol, combustion, characteristics, methanol, dual-phase

1 Introduction

Energy consumption is the stimulus for and consequence of economic development. Accordingly, as world economies grow so does the demand for energy. To meet the increased demand for energy in a sustainable manner, sources other than the conventional fossil fuels have been explored. Preferably, these should originate from bio-based or waste-based materials or even combination of both [1]. In particular cases, such combination gives way to fuels that on one side feature challenging physical and chemical properties. These properties, in general, yield detrimental effect on combustion (low calorific value, high viscosity, high water content, [2]) but on the other side, some of the properties can be exploited to improve combustion behaviour. Fostering understanding in chemical kinetics and underlying combustion phenomena namely paves the way towards tailored steering of the combustion process in a way which allows further reduction of harmful emissions compared to their fossil counterparts, while exploring specifics of these bio-based or waste-based fuels.

One of such alternatives that has had a universal appeal for minimizing environmental footprint of combustion are fuels with high oxygen content, particularly multifunctional alcohols and other similar biomass derivatives. These were already proven to significantly reduce the PM and NO_x emissions when used in gas turbines ([3-6]) and even atmospheric boilers [7]. Besides being main products from biomass conversion (i.e. pyrolysis oils, biocrudes) or even side products from production of other fuels (i.e. crude glycerine from biodiesel production) oxygenated fuels are sometimes seen as intermediates in power to gas processes, where excess CO_2 is converted to various gaseous or liquid products by the use renewable electricity, however they are almost always at an additional expense hydrogenated to exhibit properties close to fossil fuels. Both approaches are well positioned in the recent 2001/2018/EU directive as well as

49 other legislative frameworks worldwide. Hence, numerous sources of highly oxygenated
50 fuels with attractive costs exist.

51 A widely available representative of highly oxygenated waste derived fuels that have
52 several OH groups within their molecular structure is glycerol. It is highly abundant and
53 can serve well as a model compound for highly oxygenated fuels and at the same time
54 features significance in terms of its own potential to be used as a waste-derived energy
55 source [8]. Since biodiesel started to emerge as the most viable substitute for diesel fuel
56 what can be attributed to relatively simple and inexpensive transesterification process
57 of oils and fats [9] for its production, the worldwide uptake of biodiesel resulted in an
58 unprecedented amount of side-products, constituting mostly of low-quality glycerol. The
59 share of glycerol represents 10 – 20% of the weight of biodiesel produced via the
60 transesterification route [10]. With increase in biodiesel production comes a rise in
61 glycerol generation. In fact, the contribution of biodiesel process to glycerol production
62 grew from 9% in 1999 to 64% in 2009 [11].

63 Refined to high levels of purity, glycerol enjoys extensive use as raw material in food
64 and pharmaceutical industries [12]. Despite that, the recent upscale in glycerol
65 production causes a surplus in supply which results in a shortfall in its demand hence
66 its value. For instance, Yang *et al.* [13] states that the price of refined glycerol in the US
67 fell from $0.70 to $0.30 per pound in 2007 following the expansion of biodiesel
68 production; crude glycerol prices falling from $0.25 to $0.05 per pound in the same time.
69 Therefore, finding alternative value-added uses for glycerol is important as it will
70 improve the economics of the biodiesel industry as biodiesel still requires huge
71 government support to be competitive in the energy market [14].

72 Hence, the use of glycerol for power generation purposes is a highly viable option to
73 exploit large quantities that are being produced while at the same time maintiainng low

environmental footprint and increasing the energy independence of biodiesel production.

Being a fuel with challenging physical and chemical properties, particularly with its high viscosity and low calorific value, the present paper investigates a potential for drop-in application of crude glycerol in gas turbines without significant modification of the combustor with the aim of fostering understanding in chemical kinetics and underlying combustion phenomena through systematically investigating flame characteristics of highly oxygenated fuels. A continuous flow engine with extensive fuel flexibility and available in micro (<200 kW) size, the gas turbine lends itself to such investigation. However, combustion of glycerol for useful thermal power generation is unattractive. For one, its physical properties, notably high viscosity makes for inefficient flow through pipes and other narrow passageways that make up a typical fuel delivery system. This also impacts fuel atomisation – liquid spray breakup – as the flow exits a nozzle orifice; spray atomisation quality is directly related to combustion efficiency. Also, glycerol has a relatively low heating value. Typically about 16 MJ/kg, the lower heating value of glycerol is about half that of biodiesel and roughly 44% that of fossil diesel. This relatively poor energy density means a greater volume of glycerol needs to be combusted to obtain the same level of heat output as the more common fuels. Previous studies have tried to tackle these challenges by fuel preheating, use of novel nozzle designs and operating at low power output.

Crude glycerol from biodiesel synthesis by transesterification contains methanol as a major impurity and also salts, water, free fatty acids and non-glycerol organic material as minor impurities [15]. The presence of substantial amount of methanol in crude glycerol is because it is employed in excess of the required quantity in the transesterification reaction to ensure complete conversion of the reactants to biodiesel

99 [16]. Although the methanol may be recovered and reused in the process, it is not often
100 the case as it is cheaper to use a fresh supply [10], hence blending glycerol with methanol
101 for the purpose of this study correlates well also with possible realistic streams of crude
102 glycerol for combustion pruposes that requires lower degree of purification and can
103 maintain low price.

104 When reviewing the previous work done specifically on glycerol combustion,
105 fundamental combustion studies are scarce and research efforts are mostly oriented
106 towards mid to large scale setups. For example, U. S. Pharmacopeia (USP) grade glycerol
107 combustion was tested by [17] in a 7 kW prototype high-swirl burner and crude glycerol
108 in an 82 kW refractory lined furnace with NO_X emissions being 20 times higher in the
109 latter compared to the former. They also noted better performance – glycerol flames
110 were stable at higher excess air ratios compared to propane and No. 2 fuel oil. Whereas
111 the traditional fuels showed unstable combustion at equivalence ratios (ER) < 0.45, the
112 USP grade glycerol, preheated to 93°C, showed optimal combustion stability between ER
113 of 0.37 and 0.44. Jiang and Agrawal [18] tested the combustion of USP grade (with 99+%
114 purity) glycerol combustion with and without methane using a so-called flow-blurring
115 nozzle which is essentially an air-blast injector that allows a portion of the atomising
116 air into the fuel tube creating a turbulent two phase flow inside the tube and as it leaves
117 the orifice. The efficacy of this nozzle in permitting unheated straight glycerol
118 combustion was noted as was the flame structure variation with changes in fuel
119 combinations. Also, Queirós *et al.* [19] studied both the atomisation characteristics of
120 glycerol using two different air-assist atomisers and the emissions from co-combustion
121 of glycerol with natural gas and hydrogen in a laboratory furnace fired by a swirl burner.
122 With the glycerol preheated to 80°C, optimal atomiser operating conditions and the
123 influence of these conditions on post combustion emissions were noted. Muelas *et al.* [7]

using an air-assist atomiser installed in a semi-industrial furnace simulating real boiler conditions, trialled crude glycerol (preheated to 80°C) combustion as well as its blends with acetals. The blending improved the combustion behaviour of crude glycerol in terms of stability range, flame stability and CO emissions. Steinmetz *et al.* [20] investigated the particulate matter, acrolein and other volatile organic compound emissions that arising from methylated, demethylated and technical glycerol combustion; the fuels being preheated to 45°C, 120°C and 120°C respectively to reduce viscosity and facilitate pumping. Methylated glycerol referring to one with 10 – 20% methanol (b.p 65°C hence the lower preheating value) among other impurities. They used a pressure atomiser for the methylated glycerol, noting it is more commonly used in package boilers for which they envisage crude glycerol usage as fuel. The 82 kW refractory lined furnace of [17] was used for the experiments and the main conclusions were that, whereas acrolein and VOC emissions are not important, potentially corrosive particulate matter are a problem if crude glycerol with soluble catalyst is deployed in boiler applications.

Under micro-gas turbine conditions, Seljak and Katrašnik [6] investigated the combustion characteristics of glycerol in regenerative cycle mode with fuel preheating. They measured CO and THC emissions values comparable to diesel operation while simultaneously observing significantly lower NO_X and PM emissions. More recently, Rosec *et al.* [4] showed that at certain exhaust gas recirculation rates, further reduction of NO_X, CO and soot emissions can be achieved simultaneously in glycerol flames in a gas turbine burner. In the process, these studies proved the technical viability and satisfactory emissions performance of glycerol in micro-gas turbine combustion with potential application in decentralised power generation, under condition that appropriate engine adaptations, listed in [21] are implemented.

Albeit the well-known advantages of glycerol and highly oxygenated fuels in general, recognized through research performed on a highly applied level, there is currently no fundamental experimental analysis available to fully understand the role that high oxygen content has on flame shape, reaction zone properties and kinetics in the early stages of flame development. This leads to possible missed opportunities for utilization of renewable fuels with significant positive effect on emission formation. The available studies mostly cover lightly oxygenated fuels, mostly primary and secondary alcohols, while multifunctional alcohols are seldom investigated in detail.

The present study is aiming to fill this gap by for the first time systematically investigating flame characteristics of highly oxygenated fuels through CH* and OH* species chemiluminescence, supported by flame luminosity imaging. The combined data allows for an estimation and comparison of reaction zone properties like flame area, aspect ratio and lift-off height as equivalence ratio is varied. Furthermore, the study evaluates flame stability as well via analysis of temporal fluctuation of species integral intensity and via spectral analysis to confirm the capability of highly oxygenated fuels to maintain stable combustion under a wide variety of conditions. By investigating the underlying phenomena in a swirl-stabilized combustion setup, the previous efforts oriented towards applied studies in continuous combustion systems (gas turbines and furnaces) can be perfectly complemented with extensive knowledge base on flame behaviour.

2 Experimental methods and considerations

The experimental rig utilised for this study including the chemiluminescence imaging set-up is described in [22, 23]. The same fuel and air delivery and control systems were

used. The fuel injection nozzle, a standard and commercially available pressure-swirl atomiser (Delavan 0.4 GPH 60°W) was maintained as was the pressure drop of 0.85 MPa. Initial trials showed that the reaction zone length of the methanol/glycerol blends were considerably shorter than those of diesel flames. Therefore, to situate the flame well within the region of optical access of the burner, the fuel nozzle was moved upward by about 20 *mm*. This was the sole modification made to the burner set-up for the present study and allowed for the reacting flow to be captured maximally. The mixture flow rate through the nozzle was set so as to deliver an overall power output of 6 *kW* in both cases.

A schematic of the burner is shown in Fig. 1 which shows that the combustion air passes through the swirler while the liquid fuel blend is injected through the pressure-swirl nozzle which protrudes 20 mm into the burner. The axial swirler of Fig. 1 has five swirl vanes, each 2 mm thick. The tip diameter D_S is 50 mm while the hub diameter, D_H, is 16 mm. The angle of swirl, θ, is 60° so that from Eq. (1), the approximate geometric swirl number (S_N) is 1.24. Based on the geometry of the swirler, the maximum bulk exit flow velocity encountered is estimated as 2.65 m/s.

$$S_N = \frac{2}{3}\left[\frac{1-(D_H/D_S)^3}{1-(D_H/D_S)^2}\right]\tan\theta \qquad (1)$$

The chemiluminescence of two intermediate combustion species, OH* and CH*, were imaged with the viewports being different as shown in Fig. 1 because the respective filters, by virtue of being of different sizes, were fitted to different type lenses at the end of the imaging equipment. While that of the CH* filter (centred at 430 nm) was a variable focal length lens, the OH* filter (centred at 309 nm) was fitted to a lens of fixed

focal length. Both were set to be focused on the mid-plane of the combustion zone and the captured viewports are as indicated in Fig. 1.

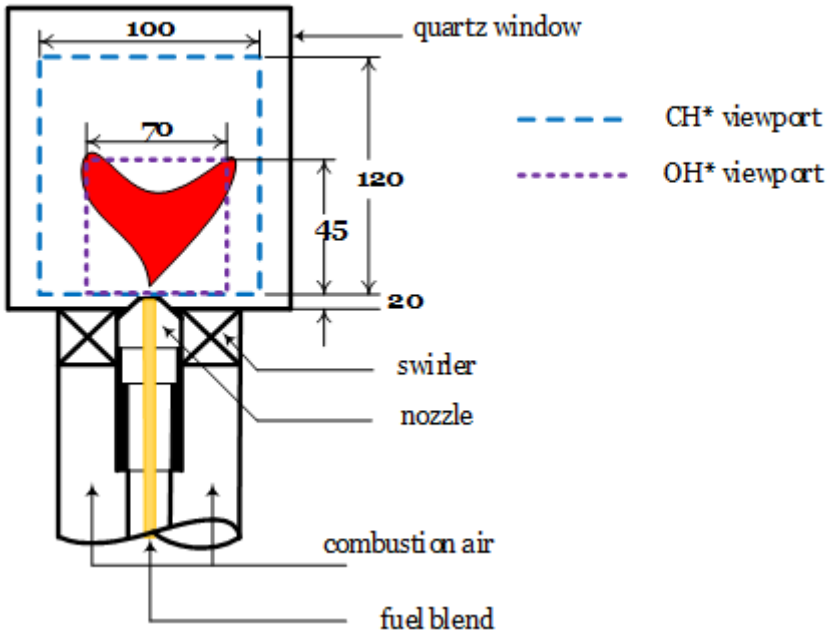

Fig. 1. Schematic of the burner set-up. Not drawn to scale and all dimensions are in *mm*.

In order to utilise the same burner upstream configuration as with the previous experiments using the set-up, the relatively high viscosity of the USP grade glycerol (see Table 1) employed had to be reduced by blending with methanol, which at the same time provides a realistic mixture, mimicking crude glycerol. However, crude glycerol has additional impurities besides methanol. According to Quispe *et al.* [10], the crude glycerol obtained from the transesterification process contains up to 70% glycerol and 20% methanol by weight; the minor impurities being salts, water, fatty acids and non-glycerol organic material. The physicochemical properties of crude glycerol are compared with commercial pure glycerol in Table 2.

212 Table 1. Selected properties of relevant fuels

Property	Diesel	Methanol	Glycerol
Approximate chemical formula	$C_{16}H_{34}$[a]	CH_4O	$C_3H_8O_3$
Lower Heating Value, LHV (*MJ/kg*)	43[b,c]	20[d]	16[f]
Density at 15^{0}C (*kg/m^3*)	850[a,b]	795[d]	1261[f]
Kinematic viscosity (*mm^2/s*) at 25^{0}C	3.50	0.59[e]	965.8[g,*]
Specific heat capacity *(KJ/kg.K)*	-	-	2.4[h]
Stoichiometric fuel-air ratio (*w/w*)	0.070	0.155	0.191

213 [a-e] refer to Refs [24-28] in that order while [f-h] refer to [6, 29, 30] accordingly.
214 *the value is reported at 20^{0}C.

215

216 Table 2. Comparison of physicochemical properties of crude glycerol and pure glycerol [31]

Property	Crude glycerol	Commercial pure glycerol
pH	9.6	6.7
Density (kg/m^3)	1.29	1.26
Flash point (^{o}C)	180	177
Fire point (^{o}C)	211	204
Carbon residue (%)	18	11.25
Ash content (%)	11.26	0.132
Solubility in water	Miscible	Miscible

217

218 Blending with methanol was necessary to circumvent glycerol preheating with its
219 associated heat loss. Previous research like some of those cited earlier utilised glycerol
220 preheating to improve pumping, atomisation and combustion efficiency raising the fuel
221 temperature to between 40^{o}C and 90^{o}C. Fig. 2 shows the amount of heat required (in
222 kW) to achieve such glycerol temperature increment for a 1 kW power output from the
223 fuel. Eq. (2) correlates power output with fuel flow rate based on its lower heating value
224 (LHV). Eq. (3) calculates the heat requirement (Q) for a desired temperature change
225 (ΔT) with c being the specific heat capacity of the liquid.

$$fuel\ flow\ rate, m\ (kg/s) = \frac{power\ output\ (kW)}{LHV\ (KJ/kg)} \quad (2)$$

226

$$Q = m\ c\ \Delta T \quad (3)$$

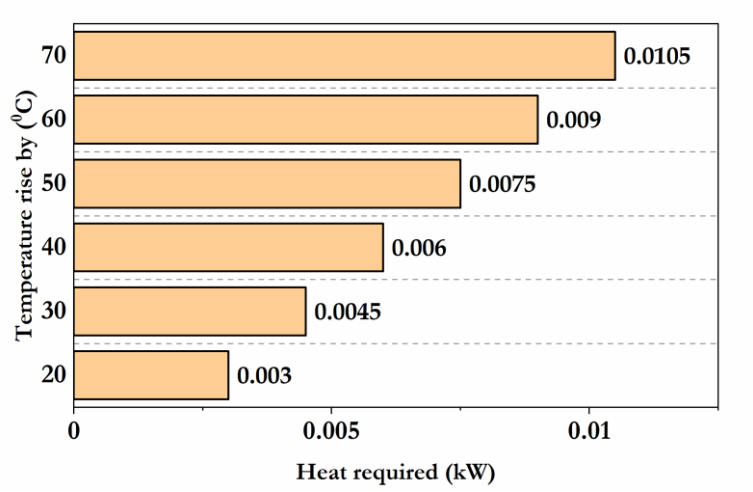

Fig. 2. Heat requirement for preheating glycerol to obtain 1 kW power from the fuel.

From Fig. 2, up to about 1% of the power output from the combustion of glycerol is spent on preheating if that is done to the levels reported in previous studies. Over and above this preheating heat loss is the heating equipment capital and maintenance cost. Besides these, preheating is associated with fuel coking problems as reported in earlier glycerol combustion studies [32, 33]. To eliminate all these negatives, the present study attained glycerol viscosity reduction by dilution with methanol rather than by fuel preheating. Also, as noted previously, methanol is major contaminant of glycerol obtained from biodiesel synthesis hence, utilising it for thinning glycerol in this case makes for a fuel blend that bears some likeness to crude glycerol earlier noted to contain up to 20% methanol. The target, then, was to generate methanol/glycerol blends with viscosities comparable to diesel at temperatures that diesel fuel may be practically utilised. This will be elaborated on in the next section after a theoretical analysis of liquid mixture viscosity determination and its temperature dependence.

3 Glycerol viscosity reduction by mixing with methanol

In gas turbines, the acceptable limits of viscosity are, in most cases, exceptionally low. Lefebvre and Ballal [34] suggest that only liquid fuels of a kinematic viscosity of up to 15 mm^2/s result in sufficient atomisation under gas turbine settings. Other authors are even more conservative. Gupta *et al.* [35] proposed a value of 12 mm^2/s while Chiaramonti *et al.* [36] and Al-Shudeifat and Donaldson [37] both recommend an even lower value of 10 mm^2/s. To fall within this limits, appropriate blending ratio of glycerol and methanol as well as mixture temperature must be defined.

Several correlations have been formulated to describe kinematic viscosity (ν) relationship with temperature (T) for liquids including the Arrhenius-type equation, the Andrade equation, the Avramov and Milchev equation and the Vogel-Fulcher-Tammann (VFT) equation. Generally, the equations take the form $\ln \nu = A + f(T)$ where $f(T)$ is an analytical function of temperature. Of these three parameter correlations, the VFT equation formulated as in Eqn. (4), has previously been found to be satisfactory in predicting the viscosity of glycerol [38], diesel [39] and methanol [40].

$$\ln \nu = A + \frac{B}{T + C} \tag{4}$$

Table 3. Fitting parameters for viscosity-temperature relationship

	A	B	C (K)
Glycerol [29]	-9.3998	2911.2	-118.2
Methanol [41]	-6.7562	2337.24	84.0853
Diesel [39]	-2.384	574.351	-140.27

In Eqn. (3), ν is the kinematic viscosity in units of mm^2/s of the liquid at temperature T in units of *Kelvin* whereas A, B and C are fitting parameters determined from several experiments. The values for these fitting parameters for the liquids considered are

267 presented in Table 3 having been taken from published literature that carried out
268 extensive analysis based on experimental data to reasonably high levels of accuracy.
269 Whereas the provided adjustable parameters leave ν in kinematic viscosity units for
270 diesel, it renders that of glycerol and methanol in dynamic viscosity units of *mPa.s*. This
271 is easily converted to kinematic viscosity by multiplying with the corresponding liquid
272 density at the particular temperature.

273 For the blends of glycerol and methanol, Chevron's mixing rule based on the concept of
274 viscosity blending index (VBI) was utilised in predicting blend viscosity. The blend
275 viscosity from the Chevron rule is a function of the volume fraction (V) of each
276 constituent of the mixture and calculated according to Eqn. (5 a-c).

$$VBI_i = \frac{\log \nu_i}{3 + \log \nu_i} \tag{5a}$$

$$VBI_{mixt.} = \sum_{i=1}^{n} V_i \times VBI_i \tag{5b}$$

$$\nu_{mixt.} = 10^{\left(\frac{3 \times VBI_{mixt.}}{1 - VBI_{mixt.}}\right)} \tag{5c}$$

277

278 The viscosity data graphed in Fig. 3 shows that a 60/40 blend of methanol/glycerol is
279 very similar to that of diesel over a wide range of temperatures. However, because the
280 intention is to utilise as much glycerol as possible, tests were carried out at 50/50 (by
281 volume) methanol/glycerol mix rationalising that it has the same viscosity at 20°C as
282 diesel at -3°C (Fig. 3). The temperature 20°C was selected as the system operates at
283 room temperature and no fuel heating occurs along the fuel lines. Also, there will be no
284 qualms burning diesel at -3°C with the existing experimental set-up. Nevertheless, in
285 the interest of equipment safety and being that glycerol/methanol use in the burner is
286 entering uncharted territory, initial tests erred on the side of caution by testing a 70/30

blend of methanol and glycerol. The results of tests on both blends are presented and discussed in the next section.

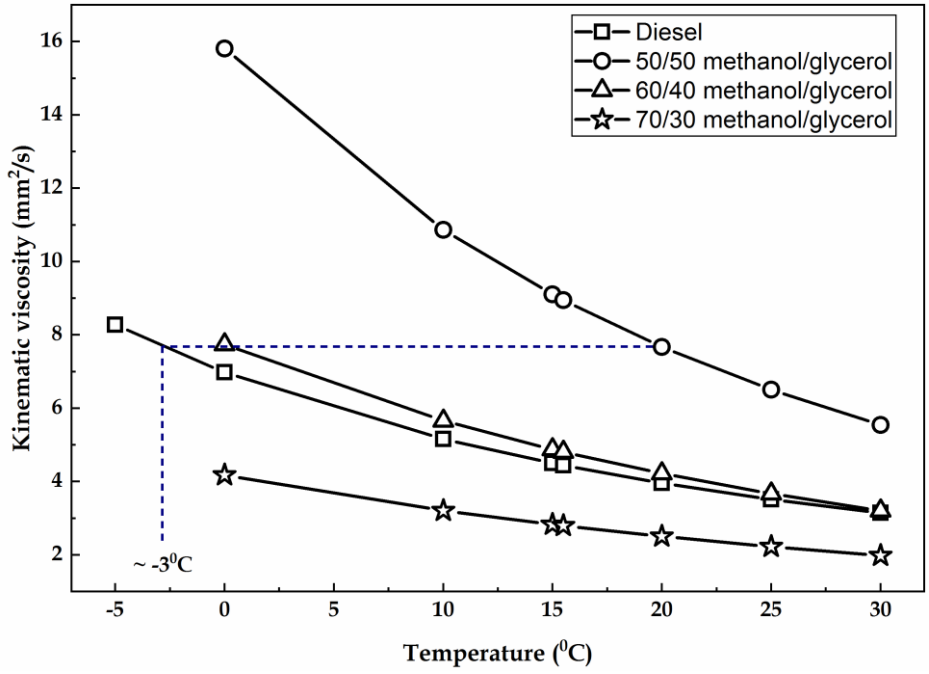

Fig. 3. Liquid and liquid mixture viscosity variation with temperature

4 Results and discussion

The results from the experiments are marshalled into three main sections. First, the flame luminosity images are presented to provide a visual rendition of the observed flame properties which is then discussed in greater detail in the next section by virtue of data obtained from CH* chemiluminescence imaging. This includes reaction zone characterisation, flame stability and spectral analyses. The last section has to do with further flame characterisation using information from OH* species chemiluminescence in order to expose the most important underlying phenomena responsible for flame behaviour.

4.1 Flame luminosity

The equivalence ratio (ER) of the flames were varied to capture the flame appearance over the widest possible stable range for both the 70/30 and 50/50 methanol/glycerol tests. Fig. 4 shows the flame luminosity images for both test cases over the identified flame stability range (between ER =0.29 and ER = 0.51).

At ER = 0.51, the 70/30 blend presents with a long narrow flame that appears to be separated from the nozzle orifice plane. This separation becomes more evident as ER increases slightly above 0.51 and eventually leads to flame blow out at ER>0.6. As air flow rate increases (decreasing ER), the 70/30 methanol/glycerol flame transitions from the narrow and separated-from-nozzle flame to a broader shape showing less separation from the nozzle. This transition point occurs at ER = 0.36.

At 0.29>ER>0.36, the flame appears to be at its stable best with no apparent changes in its shape or structure. Below ER = 0.29, however, the flame becomes flatter and highly unstable leading to lean extinction at an ER<0.23. The 50/50 case does not demonstrate the extensive variation in flame shape seen in the 70/30 case as ER changes neither does it undergo considerable lift-off prior to rich extinction. Both of these phenomena are markers of flame instability and their relative insignificance in the 50/50 flames in comparison with the 70/30 blend suggests that the greater glycerol content of the former might be causing the improvement in flame stability.

When analysing the mixture with high glycerol content (50/50) it is observable that the flattened flame shape endures into higher ERs than for the 70/30 mixture. This can be identified by the presence of the internal flame boundary, which is with 50/50 mixture very prominent at ER 0.33 and also ER 0.36 and in minor amount also at ER 0.51 while with 70/30 mixture, the internal flame boundary diminishes already with ER 0.33. This

internal boundary can be linked to the presence of flame front already within the flame cone, indicating that 50/50 mixture is capable of maintaining a conical flame shape at much higher ERs than 70/30 mixture. Additional confirmation of this phenomena can be made by observing the flame length which corresponds well to the intensity of internal flame front, resulting in elongated and finally lifted flames at high ER, where internal flame front is not present.

The described phenomena are strongly linked to central recirculation zone (CRZ) in swirl burners, which is responsible for oxygen delivery into central zone of the spray. As the 70/30 and 50/50 mixture are exhibiting a very similar stoichiometric ratio, the oxygen requirements in central flame zone are very similar, hence such prominent effect of maintaining internal flame front at low ER cannot be linked to altered air availability in the central zone. However, abundance of OH groups, being a primary centre of reactivity, resulting from higher share of glycerol in 50/50 mixture might play an important role in maintaining the flame front also in areas with low air availability that occur at high ER.

Tracing these observations back to the fuel's physical and chemical properties, it would be expected that aggravated mixture formation caused by high viscosity of glycerol would result in delayed flame onset and also possible flame lift-off, however this does not occur. Similar results were observed also in combustion of glycerol and other highly oxygenated fuels in a realistic gas turbine combustion setup, where stable flames appeared very close to the injection nozzle [21, 32, 42], requiring additional thermal protection of the nozzle.

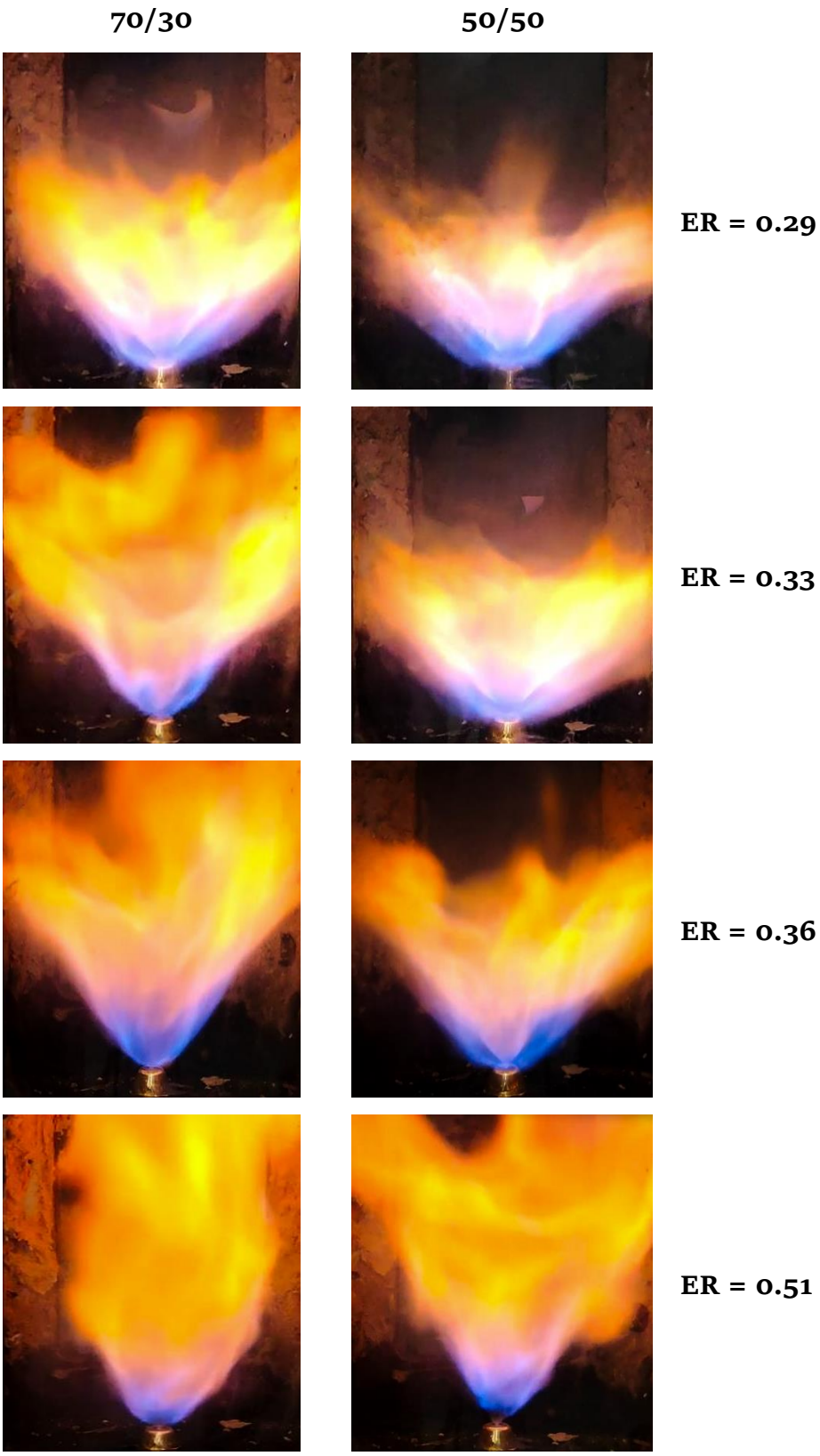

Fig. 4. Methanol/glycerol flame luminosity at different equivalence ratios

354 The maximum flame temperature in each blend of methanol/glycerol tested was
355 estimated using ANSYS Chemkin equilibrium model. The results are shown in
356 Fig. 5 and compared with diesel flame equilibrium temperatures with the species
357 $C_{16}H_{34}$ used as diesel surrogate. Over a wide range of both rich and lean ERs,
358 including the range of equivalence ratios for the methanol/glycerol blends tested
359 in this work (shaded in Fig. 5), the equilibrium temperature is highest in the
360 50/50 case and lowest in the diesel case. This trend of maximum flame
361 temperatures reflects the inherent oxygen content of the fuels. Diesel, for
362 instance, will require more oxygen hence more air for its combustion than the
363 oxygenated fuel blends. The nitrogen component of air acts as a diluent so that
364 flame temperatures decrease as air (therefore nitrogen) requirement increases.
365 The higher attainable flame temperatures in methanol/glycerol flames compared
366 to diesel should not be of concern in the context of potentially higher NO_X
367 emissions because stable methanol/glycerol flames occur at ERs less than 0.4. At
368 such ERs, the maximum flame temperatures of the methanol/glycerol (from Fig.
369 5) are well below those of stable diesel flames (for example, ER = 0.7 in [22])
370 that are associated with relatively low NO_X emissions.

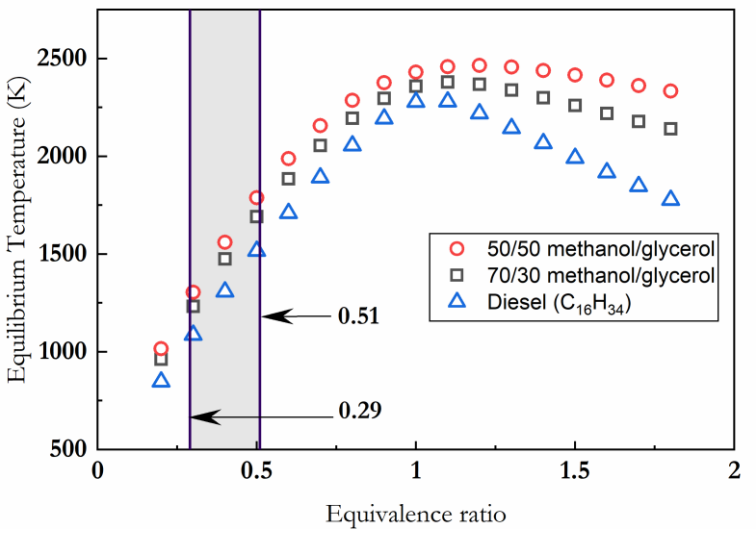

371

372 Fig. 5. Equilibrium flame temperature at different ERs for 50/50 and 70/30 methanol/glycerol
373 blends and diesel modelled as $C_{16}H_{34}$.

374

375 **4.2 CH* species chemiluminescence**

376 In order to investigate this phenomenon further, the CH* species chemiluminescence
377 from 70/30 and 50/50 methanol/glycerol flames are presented, highlighting the species
378 distribution and reacting flow dynamics using CH* chemiluminescence.

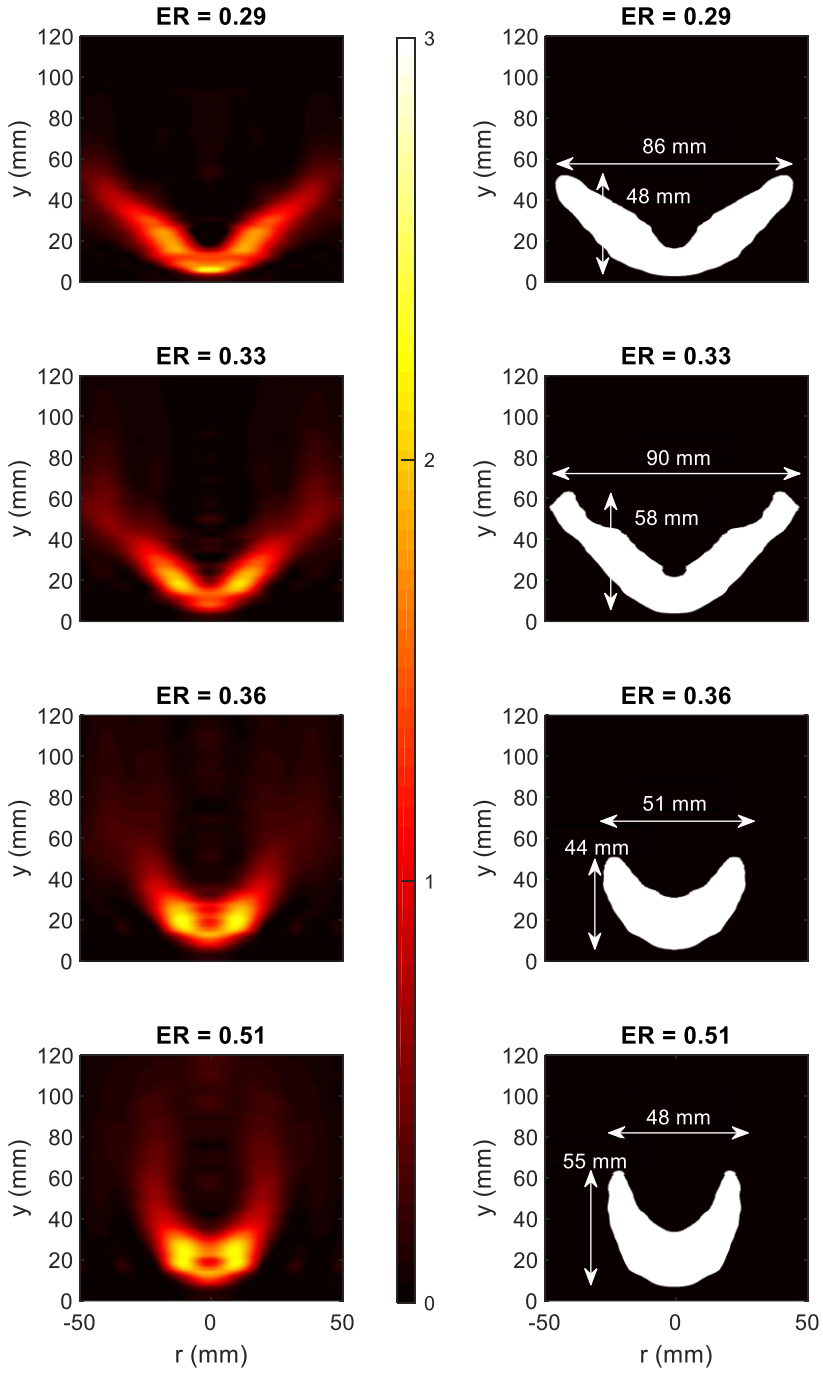

379 Fig. 6. Left column: Abel deconvoluted chemiluminescence images of CH* species in 70/30
380 methanol/glycerol flames at different equivalence ratios. Right column: Corresponding binary
381 images. Flow is from top to bottom.

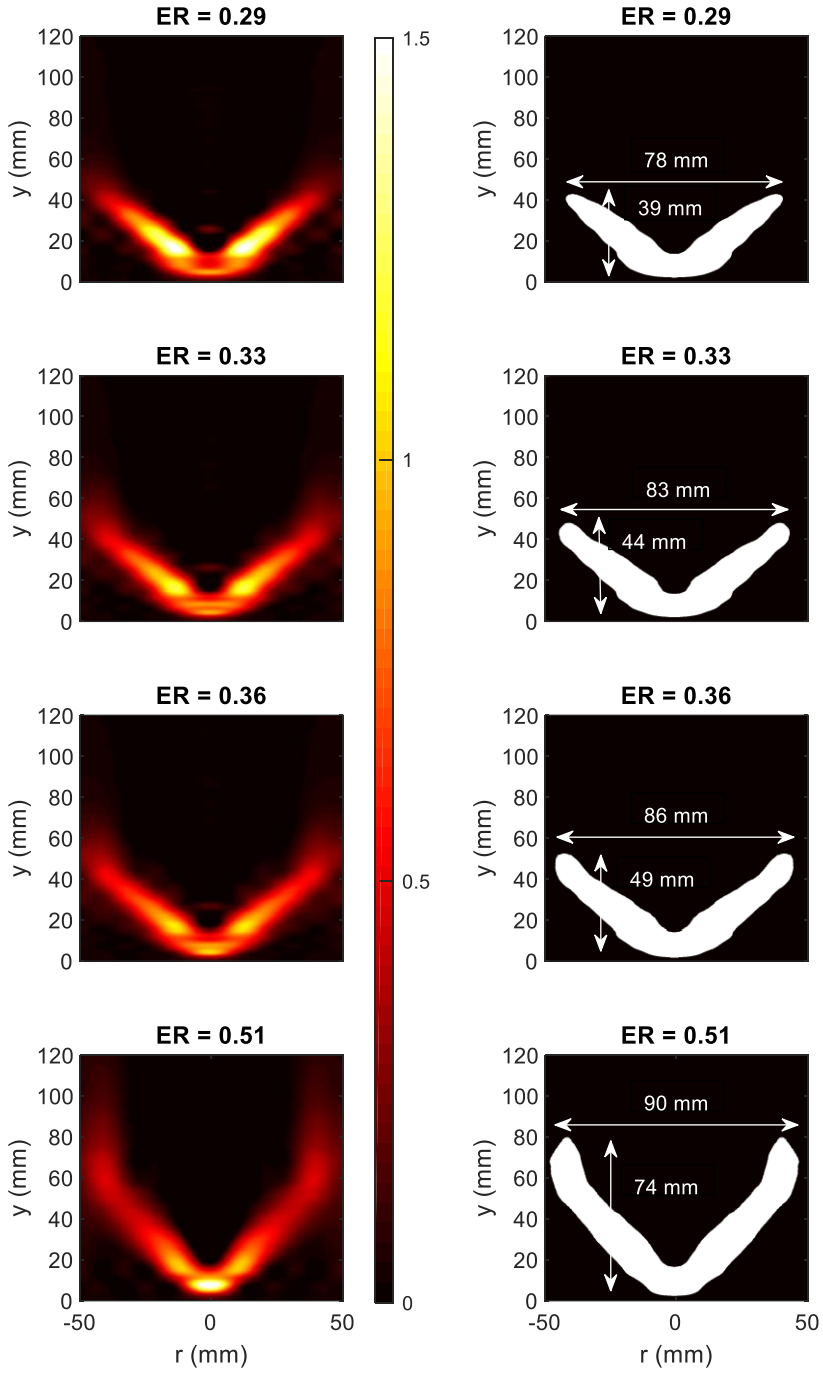

382 Fig. 7. Left column: Abel deconvoluted chemiluminescence images of CH* species in 50/50
383 methanol/glycerol flames at different equivalence ratios. Right column: Corresponding binary
384 images. Flow is from top to bottom.

385

386

387

Fig. 6 shows the 70/30 methanol/glycerol flame CH* chemiluminescence whereas Fig. 7 displays that of the 50/50 blend for corresponding ERs. Each figure is accompanied by a binary equivalent obtained from MATLAB processing. Similar to Agwu *et al.* [23], MATLAB's Otsu thresholding method was used to determine which pixels are designated white or black. The Otsu thresholding method is suitable here because it selects a threshold value that minimises the intraclass variance of the black and white pixels. The threshold value was determined for the ER = 0.29 case and applied to all the other cases. With obtained data, the reaction zone properties can be further investigated.

4.2.1 Reaction zone properties

In addition to the reaction zone area and reaction zone aspect ratio (width/height), the variability in flame lift-off height has been highlighted in Fig. 8. As shown in the binary images of the last two figures, the reaction zone length is estimated as the distance between the uppermost and lowermost unity pixels whereas the reaction zone width is represented by the distance between the unity pixels at the lateral edges of the binary image. The reaction zone area is modelled as the sum of the unity pixels in the binary image while the flame lift-off height is considered to be the vertical distance, in the binary image, from the lowermost unity pixel to the $y = 0$ point on the image.

Fig. 6 shows that a 70/30 blend of methanol and glycerol generates flames whose reaction zone properties vary widely as equivalence ratio is altered compared to a 50/50 blend of the same fuels. This observation is consistent with the flame luminosity images in which flame shape was noted to vary much more significantly with changes in ER for the 70/30 blend than for the 50/50 blend. Also, there was appreciable flame lift-off especially at the higher end of the ER range for the 70/30 case relative to the 50/50 case and this, again, is in agreement with the data obtained from flame luminosity images.

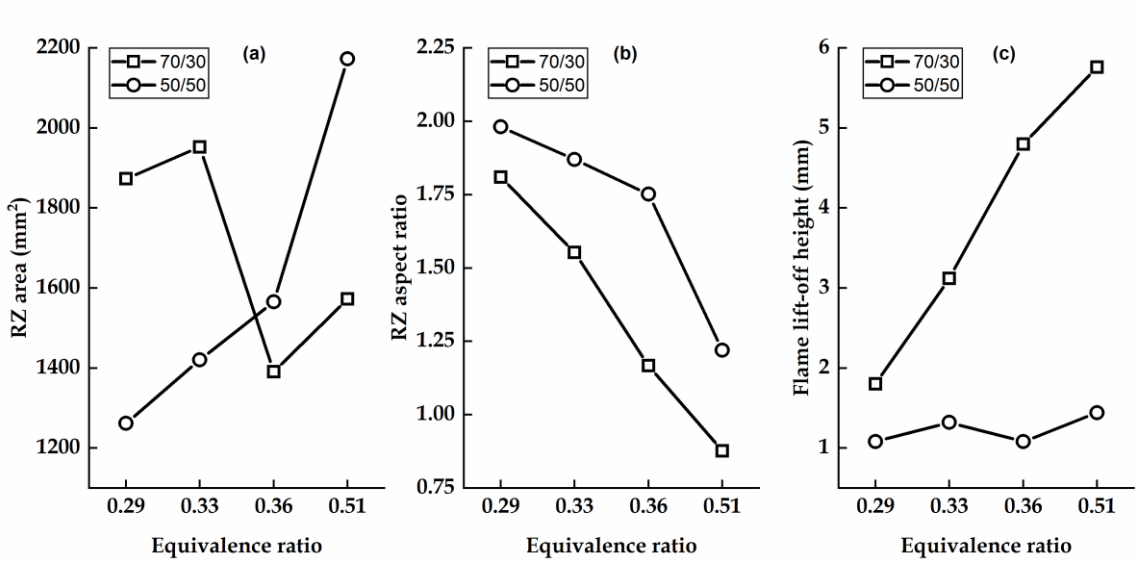

Fig. 8. Reaction zone (RZ) properties of methanol/glycerol blends.

The reaction zone data confirms the hypothesis that oxygen content in the fuel alone is not a sufficient marker to describe the combustion properties of highly oxygenated fuels and that higher alcohols with larger number of OH groups indeed exhibit increased resistance towards rich extinction. At the same time, they are capable of maintaining stable flames also under highly diluted conditions as previously shown by stable lift-off height over a wide range of ER and less pronounced trend of RZ area increase with 50/50 blends.

4.2.2 Flame Stability

In order to further analyse the stability of methanol/glycerol flames, analysis based on methodology as in [23, 24] was carried out. The idea is to sum up the CH* species chemiluminescence intensity for each of the 250 captured images and observe the temporal variation of each sum with the overall average intensity. The degree of variation of intermediate combustion species intensity over the capture period being indicative of flame stability. Put differently, the lesser the variation of the species

intensity about the average value over time, the greater the flame stability and vice versa.

From the data obtained, the average CH* species chemiluminescence intensity for the 250 images does not appear to vary very much as ER changes in each of the two test categories so standard deviation could be used for species intensity temporal variability comparison. However, across the two categories of tests (i.e. 70/30 and 50/50), there is a greater variation in the average CH* species chemiluminescence intensity. Consequently, to enable a fair comparison of both sets of tests, coefficient of variation, *CoV* (standard deviation of a set of data normalised by its mean) has been used. This comparison is shown in Fig. 9. Comparing the blends individually, it is observed that flame stability steadily improves – albeit marginally – as ER increases. Juxtaposing the two blends, it is seen that the 50/50 blend of methanol/glycerol generates flames that are of greater stability than the 70/30 blend across the range of stable flame operation of the fuels – which further confirms the observations of the flame luminosity and the chemiluminescence analysis.

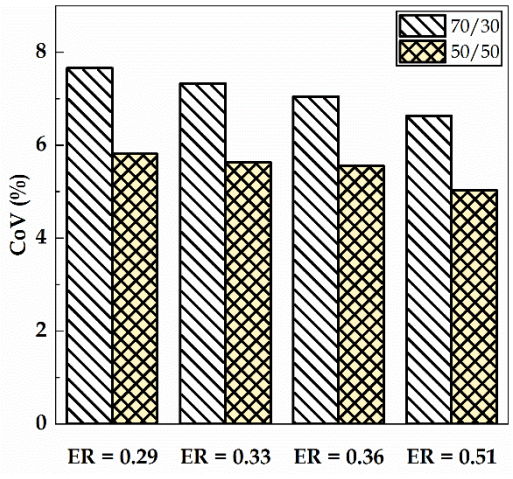

Fig. 9. CH* species chemiluminescence CoV for 70/30 and 50/50 methanol glycerol flames

4.2.3 Spectral analysis

Additional insight into flame stability can be obtained by analysing the CH* radical intensity fluctuation and its corresponding magnitude by scaling it to a different domain. In Fig. 9 for the 70/30 blend and Fig. 10 for the 50/50 blend, the time series data for the CH* intensity signals were converted by means of fast Fourier transform (FFT) to a frequency-domain signal. While time-domain analysis shows how a signal changes over time, frequency-domain analysis shows how the signal's energy is distributed over a range of frequencies. Both figures are plotted to the same scale for ease of comparison. The chemiluminescence data sample size was 250 with the sampling time interval being 0.1s so the FFT sampling frequency was set as 25 samples per second. Half of this sampling frequency is plotted to avoid duplication of FFT representation. Also, in order to improve FFT accuracy, instead of using 128 of the 250 data points, six additional points were included making a total of 256. These additional data were selected as the average of the 250 others in each case.

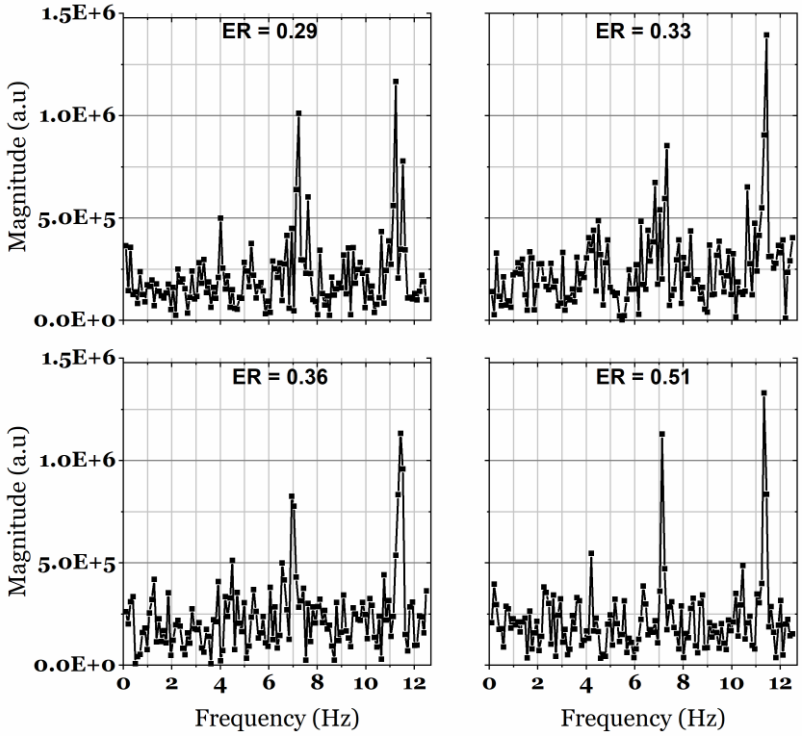

Fig. 10. FFT plots of CH* species chemiluminescence intensity for 70/30 methanol/glycerol flame at different ERs.

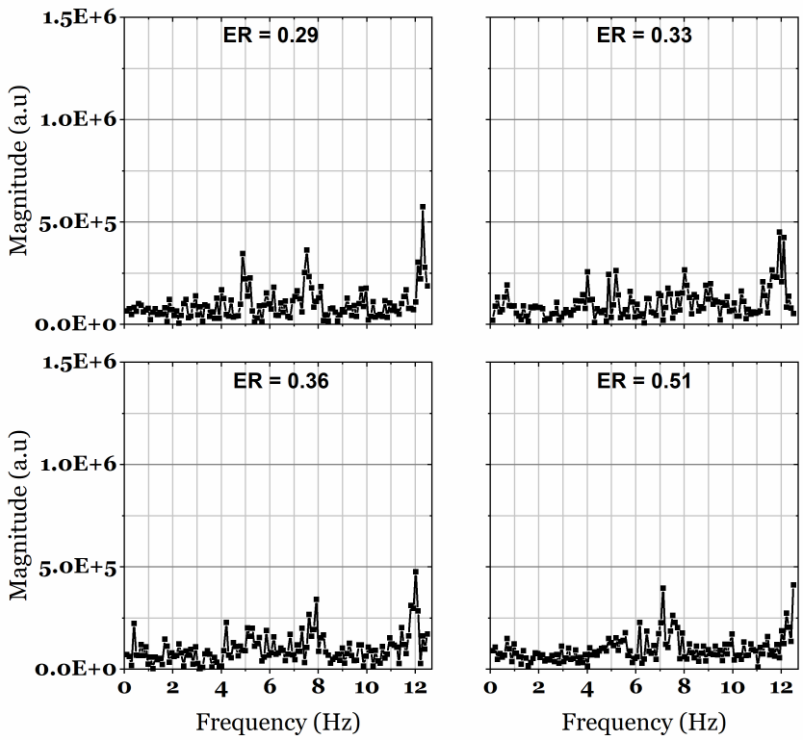

Fig. 11. FFT plots of CH* species chemiluminescence intensity for 50/50 methanol/glycerol flame at different ERs.

Spectral lines that are out of proportion with others in the frequency domain representation of signals indicate signal periodicity – alternating periods of high and low signal intensity. In this case, it is likely a result of increased flame flickering as observed in the 70/30 case compared with the 50/50 case. Also, Mondal *et al.* [43] noted that diffusion flame flickering as opposed to pressure fluctuations was responsible for low frequency bands observed in flames in a similar burner. Comparing Fig. 10 and Fig. 11 then, there is an attenuation of the magnitudes in signal amplitudes in the latter in relation to the former indicating greater flame flickering hence higher heat release rate fluctuation in the 70/30 case than in the 50/50 blend. Therefore, in the two glycerol/methanol blends tested, flame stability is higher in the 50/50 blend. This

observed improvement in flame stability is consistent with the statistical analysis shown in Fig. 9 and again confirms that notwithstanding its challenging physical and chemical properties, higher share of glycerol in the analysed mixtures yields greater flame stability and offers the opportunity to extend the operating space on both ends of analysed ER interval.

4.3 OH* species chemiluminescence

To further evaluate the flame behaviour and identify the possible role of large abundance of OH groups in multifunctional alcohols and highly oxygenated fuels in general, the OH* chemiluminescence images are shown in Fig. 11 with the 70/30 methanol/glycerol blend to the left and the 50/50 blend to the right. As earlier noted, the end of the imaging equipment used for the OH* species chemiluminescence measurement was different from that employed for CH* acquisition hence the different image scales (comparing Fig. 12 with Fig. 6 and 7). Because of the narrower and shorter field of view obtained for OH* and because the flame brush varies widely with changes in ER, analysing the reaction zone characteristics in the manner done using CH* distribution would be spurious. Therefore, extensive analysis of OH* species chemiluinescence in the context of these parameters is not carried out.

However, the peculiar image resolution obtained for the OH* species capture zooms in on the primary zone of combustion where OH* species are known to be most concentrated. The OH* species distribution within this zone as shown in Fig. 12 shows moderate consistency with the CH* species distribution and the flame luminosity images. For instance, in the 70/30 case at ER = 0.51 and partly also at ER=0.36, OH* species are observed to be concentrated in a narrow cone in the near-nozzle region with

503 gradual transition, which corresponds to absence of the internal flame front as discussed
504 in section 4.1. As ER decreases, the species increasingly spreads away from the centre
505 of the burner towards the edges and appears to separate at the centre in the ER = 0.29
506 case what is again consistent with strong central recirculation zone. For the 50/50
507 blend, similar to the CH* species, OH* species do not form a ball in the ER = 0.51 flame
508 which gradually splits as ER decreases. Instead, and conforming to the CH* species
509 distribution, the OH* species intensity concentration is the most noticeable variation –
510 certainly from a qualitative standpoint – as ER changes.

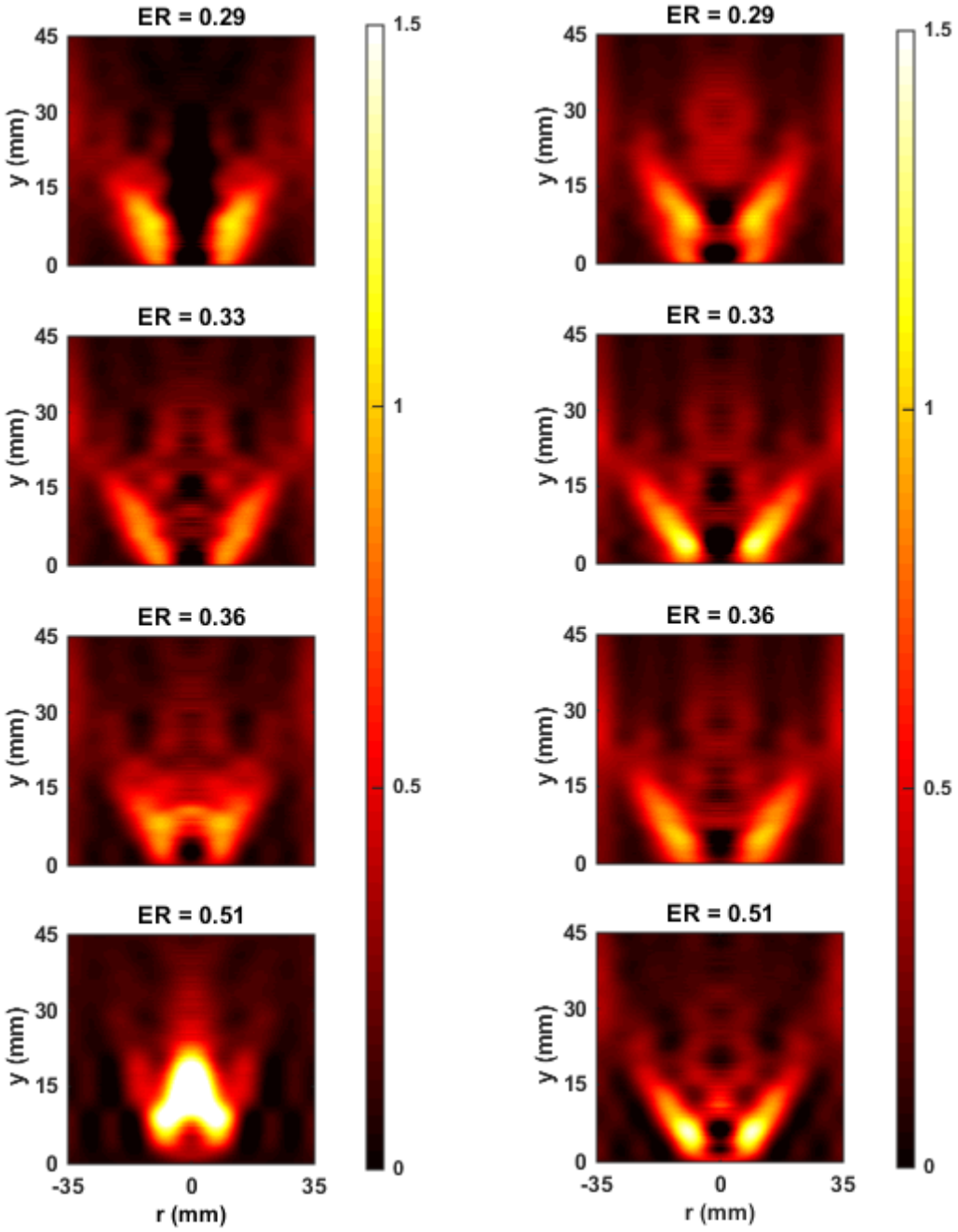

Fig. 12. Abel deconvoluted chemiluminescence images of OH* species in 70/30 methanol/glycerol flames (left column) and 50/50 50 methanol/glycerol flames (right column) at different equivalence ratios. Flow is from top to bottom.

Further, it is instructive to note that, whereas only a fraction of the CH* viewport is captured in the OH* species imaging (see Fig. 1), it appears that the captured region is where majority of the OH* species are concentrated. And apart from the ER = 0.51 flame in the 70/30 case, a greater concentration of the OH* species occurs below the y = 15

mm plane than above it. This is definitely not the case for the CH* species distribution the concentration of which is not significant below the y = 15 mm plane as it is above that plane. The implication of this is that in the highly oxygenated fuel blends tested, OH*-forming reactions occur earlier than CH* synthesizing reactions. The OH* radical in hydrocarbon combustion is mainly generated via two reactions: : $CH + O_2 \rightarrow CO + OH^*$ $(R1)$ and $H + O + M \rightarrow OH^* + M$ $(R2)$, however it can be generated via numerous pathways that depend on structure and molecular weight of alcohols. Particularly when examining the secondary alcohols, the reaction with the greater influence in hydrocarbon flames is R1 [44]. However, based on the earlier observation from the chemiluminescence images in which OH* appears well before CH*, the dominating reaction in OH* generation in the combustion of the highly oxygenated fuel blend in the present study is reaction R2. Reaction R1 must be weakened because it requires CH as a reactant which, based on the chemiluminescence images, is not significantly present in the region where OH* is concentrated. The dominant reaction (R2) involves dissociation of molecular oxygen into atomic oxygen and because it occurs relatively early in the reacting flow, the oxidation reaction needed for combustion will require more molecular oxygen. Consequently, lower equivalence ratios are encountered in highly oxygenated fuel combustion compared with non-oxygenated hydrocarbon combustion.

Particularly in glycerol, initiation reactions involve either the cleavage of a C-C bond or the cleavage of C-O terminal bond with formation of primary radicals. However, propagation relies on heavily on H abstraction reactions which are reported to be influenced by OH groups. The reported reaction rate for H abstraction from alpha carbon atoms (primary as well as secondary) is almost 50% higher than the rate values of the H abstraction from alkanes [45], what is contributed to a presence of OH group on the same carbon atom which significantly promotes the H abstraction and consequent

propagation reactions lead to relatively fast availability of H atoms, necessary for R2 mentioned above that leads to fast formation of OH. By having three major centres of reactivity (one on each carbon atom), the glycerol as well as other multifunctional alcohols exhibit a highly interesting combustion behaviour.

Based on the analysed results and under consideration that glycerol is a fuel with highly challenging physical and chemical properties and its high reactivity might go unnoticed, the presented analysis exhibits significant opportunity to exploit the unique properties of such fuels. These could support several combustion processes that rely on highly diluted mixtures where mixture ignition might be challenging. As such highly oxygenated fuels could play an important role when implemented into latest innovative combustion concepts that rely on large EGR ratios (for example flameless combustion regimes), or as an initializing component to support combustion of fuels featuring low reactivity, where highly oxygenated fuels with large number of OH might play a beneficial role as an ignition improvers.

5. Conclusion

With highly oxgenated fuels being one of the major opportunities for low-emission power generation, the paper for the first time provides a fundamental analysis of flame related phenomena on the case of highly relevant representative fuel blend. As interest in biodiesel production and its utilisation in combustion system grows, so does the production of crude glycerol, mixed with substantial amounts of excess methanol. To simulate highly oxygenated fuels and simultaneously address crude glycerol combustion properties, methanol was blended with pure glycerol and tested as fuel in a model swirl-stabilised gas turbine combustor. A 70/30 blend of methanol and glycerol as well as a

50/50 blend was combusted in the model burner with only minor modification of the set-up. The main findings from the study can be summed as follows:

1. Mixing methanol with glycerol improves the viscosity of glycerol and a 60/40 (by volume) blend of methanol/glycerol has very similar viscosity to diesel over a practical temperature range.
2. Lean and rich flame extinction range for 70/30 (by volume) and 50/50 methanol/glycerol blends occurs at low equivalence ratios (approximately 0.2 – 0.6), what confirms the increased combustion stability of highly oxygenated fuels under lean conditions.
3. A 50/50 blend of methanol/glycerol shows greater flame stability compared with a 70/30 methanol/glycerol blend as evidenced by flame luminosity and CH* species chemiluminescence images, exposing the beneficial role of multifunctional alcohols.
4. Analysis of OH species reveal a beneficial role of high reaction rate of H-abstraction reactions that are responsible for flame propagation, leading to suggestions that highly oxygenated fuels might play an important role as combustion initiating components in multi-fuel processes.

Conclusively, on the basis of the findings in the present study and capability of stable combustion in substantially lean conditions, glycerol as well as other highly oxygenated fuels merits consideration for use as fuel in novel combustion concepts with high dilution rates or as a support fuel in reactivity controlled combustion. At the same time, the study confirms that standalone power generation with glycerol alongside small and medium scale decentralised biodiesel production plant is possible, given the prerequisite that the content of minor inorganic contaminants is reduced to acceptable limits.

Acknowledgement

We are grateful to Mr. Malcolm Seaborne and the rest of the technical staff in Cardiff University's Thermofluids Lab for their help in setting up the experimental rig. Ogbonnaya Agwu is grateful to the Petroleum Technology Development Fund (PTDF) for sponsoring his PhD studies at Cardiff University. The authors also acknowledge the financial support from the Slovenian Research Agency (research core funding No. P2-0401 – Energy engineering and project funding Z2-1862 – Zero footprint combustion for green energy generation).

References

[1] Raes J, Brekelmans H, Hieminga G, van Dun J, Bani M, Cracau A, Rooms D, Piechocki R, and Naber G. *Circular Economy Finance Guidelines*. 2018.

[2] Seljak T, Buffi M, Valera-Medina A, Chong CT, Chiaramonti D, and Katrašnik T. *Bioliquids and their use in power generation – A technology review.* Renewable and Sustainable Energy Reviews, 2020. **129**.

[3] Buffi M, Seljak T, Cappelletti A, Bettucci L, Valera-Medina A, Katrašnik T, and Chiaramonti D. *Performance and emissions of liquefied wood as fuel for a small scale gas turbine.* Applied Energy, 2018. **230**: p. 1193-1204.

[4] Rosec Ž, Katrašnik T, Žvar Baškovič U, and Seljak T. *Exhaust gas recirculation with highly oxygenated fuels in gas turbines.* Fuel, 2020. **278**: p. 118285.

[5] Rosec Ž, Dias V, Contino F, Katrašnik T, and Seljak T. *Comparative analysis of bio-intermediates and waste-derived fuels in experimental gas turbine.* Frontiers in Mechanical Engineering, 2020. **6**: p. 71.

[6] Seljak T and Katrašnik T. *Emission reduction through highly oxygenated viscous biofuels: Use of glycerol in a micro gas turbine.* Energy, 2019. **169**: p. 1000-1011.

[7] Muelas A, Remacha P, Pina A, Barroso J, Sobrino A, Aranda D, Bayarri N, Estévez C, and Ballester J. *Combustion of crude glycerol and its blends with acetals.* Experimental Thermal and Fluid Science, 2020. **114**.

[8] He Q, McNutt J, and Yang J. *Utilization of the residual glycerol from biodiesel production for renewable energy generation.* Renewable and Sustainable Energy Reviews, 2017. **71**: p. 63-76.

[9] Ogunkunle O and Ahmed NA. *A review of global current scenario of biodiesel adoption and combustion in vehicular diesel engines.* Energy Reports, 2019. **5**: p. 1560-1579.

[10] Quispe CAG, Coronado CJR, and Carvalho Jr JA. *Glycerol: Production, consumption, prices, characterization and new trends in combustion.* Renewable and Sustainable Energy Reviews, 2013. **27**: p. 475-493.

[11] Ayoub M and Abdullah AZ. *Critical review on the current scenario and significance of crude glycerol resulting from biodiesel industry towards more sustainable renewable energy industry.* Renewable and Sustainable Energy Reviews, 2012. **16**(5): p. 2671-2686.

[12] Chozhavendhan S, Karthiga Devi G, Bharathiraja B, Praveen Kumar R, and Elavazhagan S, *Assessment of crude glycerol utilization for sustainable development of biorefineries*, in *Refining Biomass Residues for Sustainable Energy and Bioproducts*. 2020. p. 195-212.

[13] Yang F, Hanna MA, and Sun R. *Value-added uses for crude glycerol - a byproduct of biodiesel production.* Biotechnology for Biofuels, 2012. **5**(13).

[14] Ajanovic A and Haas R. *Economic challenges for the future relevance of biofuels in transport in EU countries.* Energy, 2010. **35**(8): p. 3340-3348.

[15] Sivasankaran C, Ramaujam PR, Balasbramanian B, and Mani J. *Recent progress on transforming crude glycerol into high value chemicals: a critical review.* Biofuels, 2019. **10**(3): p. 309-314.

[16] Sdrula N. *A study using classical or membrane separation in the biodiesel process.* Desalination, 2010. **250**(3): p. 1070-1072.

[17] Bohon MD, Metzger BA, Linak WP, King CJ, and Roberts WL. *Glycerol combustion and emissions.* Proceedings of the Combustion Institute, 2011. **33**(2): p. 2717-2724.

[18] Jiang L and Agrawal AK. *Combustion of straight glycerol with/without methane using a fuel-flexible, low-emissions burner*. Fuel, 2014. **136**: p. 177-184.

[19] Queirós P, Costa M, and Carvalho RH. *Co-combustion of crude glycerin with natural gas and hydrogen.* Proceedings of the Combustion Institute, 2013. **34**(2): p. 2759-2767.

[20] Steinmetz SA, Herrington JS, Winterrowd CK, Roberts WL, Wendt JOL, and Linak WP. *Crude glycerol combustion: Particulate, acrolein, and other volatile organic emissions.* Proceedings of the Combustion Institute, 2013. **34**(2): p. 2749-2757.

[21] Seljak T, Pavalec K, Buffi M, Valera-Medina A, Chiaramonti D, and Katrašnik T. *Challenges and Solutions for Utilization of Bioliquids in Microturbines.* Journal of Engineering for Gas Turbines and Power, 2018. **141**(3).

[22] Agwu O and Valera-Medina A. *Diesel/syngas co-combustion in a swirl-stabilised gas turbine combustor.* International Journal of Thermofluids, 2020. **3-4**.

[23] Agwu O, Runyon J, Goktepe B, Chong CT, Ng J-H, Giles A, and Valera-Medina A. *Visualisation and performance evaluation of biodiesel/methane co-combustion in a swirl-stabilised gas turbine combustor.* Fuel, 2020. **277**.

[24] Chong CT and Hochgreb S. *Flame structure, spectroscopy and emissions quantification of rapeseed biodiesel under model gas turbine conditions.* Applied Energy, 2017. **185**: p. 1383-1392.

[25] Li Z, Wang Y, Geng H, Zhen X, Liu M, Xu S, and Li C. *Effects of diesel and methanol injection timing on combustion, performance, and emissions of a diesel engine fueled with directly injected methanol and pilot diesel.* Applied Thermal Engineering, 2019. **163**.

[26] Wang Y, Wang H, Meng X, Tian J, Wang Y, Long W, and Li S. *Combustion characteristics of high pressure direct-injected methanol ignited by diesel in a constant volume combustion chamber.* Fuel, 2019. **254**.

[27] Zhen X, Li X, Wang Y, Liu D, and Tian Z. *Comparative study on combustion and emission characteristics of methanol/hydrogen, ethanol/hydrogen and methane/hydrogen blends in high compression ratio SI engine.* Fuel, 2020. **267**.

[28] Duraisamy G, Rangasamy M, and Govindan N. *A comparative study on methanol/diesel and methanol/PODE dual fuel RCCI combustion in an automotive diesel engine.* Renewable Energy, 2020. **145**: p. 542-556.

[29] Ferreira AGM, Egas APV, Fonseca IMA, Costa AC, Abreu DC, and Lobo LQ. *The viscosity of glycerol.* The Journal of Chemical Thermodynamics, 2017. **113**: p. 162-182.

[30] EngineeringToolbox. *Specific Heat of some liquids and fluids*. Available from: https://www.engineeringtoolbox.com/specific-heat-fluids-d_151.html. accessed: May 15, 2020.

[31] Chozhavendhan S, Kumar RP, Sivarathnakumar S, Arulraj JV, Elavazhagan S, Bharathirja B, and Varjani SJ. *Production of ethanol by Zymomonas mobilis using partially purified glycerol*. Journal of Energy and Environmental Sustainability, 2017. **4**: p. 15-19.

[32] Seljak T, Širok B, and Katrašnik T. *Advanced fuels for gas turbines: Fuel system corrosion, hot path deposit formation and emissions.* Energy Conversion and Management, 2016. **125**: p. 40-50.

[33] Seljak T and Katrašnik T. *Designing the microturbine engine for waste-derived fuels.* Waste Management, 2016. **47**: p. 299-310.

[34] Lefebvre AH and Ballal DR. *Gas Turbine Combustion: Alternative fuels and emissions*. 3rd ed. 2010: CRC Press Taylor & Francis Group.

[35] Gupta KK, Rehman A, and Sarviya RM. *Bio-fuels for the gas turbine: A review.* Renewable and Sustainable Energy Reviews, 2010. **14**(9): p. 2946-2955.
[36] Chiaramonti D, Oasmaa A, and Solantausta Y. *Power generation using fast pyrolysis liquids from biomass.* Renewable and Sustainable Energy Reviews, 2007. **11**(6): p. 1056-1086.
[37] Al-Shudeifat MA and Donaldson AB. *Combustion of waste trap grease oil in gas turbine generator.* Fuel, 2010. **89**(3): p. 549-553.
[38] Yadav A, Trivedi S, Rai R, and Pandey S. *Densities and dynamic viscosities of (choline chloride+glycerol) deep eutectic solvent and its aqueous mixtures in the temperature range (283.15–363.15)K.* Fluid Phase Equilibria, 2014. **367**: p. 135-142.
[39] Yuan W, Hansen AC, Zhang Q, and Tan Z. *Temperature-dependent kinematic viscosity of selected biodiesel fuels and blends with diesel fuel.* Journal of the American Oil Chemists' Society, 2005. **82**(3): p. 195-199.
[40] Gülüm M and Bilgin A. *A comprehensive study on measurement and prediction of viscosity of biodiesel-diesel-alcohol ternary blends.* Energy, 2018. **148**: p. 341-361.
[41] DDB. Available from: http://ddbonline.ddbst.de/VogelCalculation/VogelCalculationCGI.exe. accessed: April 6, 2020.
[42] Seljak T, Rodman Oprešnik S, Kunaver M, and Katrašnik T. *Wood, liquefied in polyhydroxy alcohols as a fuel for gas turbines.* Applied Energy, 2012. **99**: p. 40-49.
[43] Mondal S, Mukhopadhyay A, and Sen S. *Dynamic Characterization of a Laboratory-Scale Pulse Combustor*. Combustion Science and Technology, 2014. **186**(2): p. 139-152.
[44] Ballester J and García-Armingol T. *Diagnostic techniques for the monitoring and control of practical flames.* Progress in Energy and Combustion Science, 2010. **36**: p. 375-411.
[45] Hemings EB, Cavallotti C, Cuoci A, Faravelli T, and Ranzi E. *A Detailed Kinetic Study of Pyrolysis and Oxidation of Glycerol (Propane-1,2,3-triol).* Combustion Science and Technology, 2012. **184**(7-8): p. 1164-1178.